32nd URSI GASS, Montreal, 19–26 August 2017

A spacetime adaptive approach to characterize complex dispersive media

Reza Abedi*(1), Saba Mudaliar(2)
(1) University of Tennessee Space Institute (UTSI), Tullahoma, TN, 37355, www.rezaabedi.info, rabedi@utsi.edu
(2) Sensors Directorate, Air Force Research Laboratory, Wright-Patterson AFB, Dayton, OH 45433, saba.mudaliar@us.af.mil

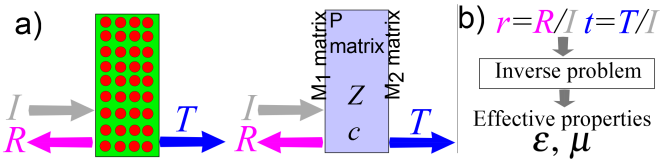

Figure 1. Schematic of parameter retrieval method to derive effective properties from scattering parameters.

Abstract

We present a time domain approach that can obtain reflection and transmission coefficients of a material for a wide range of frequencies. The advanced method of spacetime discontinuous Galerkin method is used to obtain the time domain response of a unit cell to an incident wave. Adaptive operations in space and time permits very efficient and accurate tracking of wave fronts. By Fourier analysis and inversion of the obtained transmission and reflection coefficients in the frequency domain, we obtain equivalent impedance, wave speed, permittivity, and permeability of the unit cell for the given frequencies. The linear solution cost of the SDG method, its powerful adaptive operations, and derivation of the entire spectrum with one time domain simulation are attractive attributes of the proposed method.

1 Introduction

1.1 Parameter retrieval method

Figure 1 depicts the schematic of parameter retrieval method. If a uniform medium of given impedance Z, wave speed c, and thickness l is sandwiched between an ambient medium with electrical permittivity ε_0 and magnetic permeability μ_0 we can calculate its reflection and transmission coefficients for any given frequency. Now, if a complex media such as the one shown on the left is given we can calculate its transmission and reflection coefficients and look for effective Z and c that would result in the same scattering coefficients. These values are subsequently used to obtain effective material properties for the complex media by solving an inverse problem as shown in fig. 1b). The scattering parameters are often obtained by a frequency domain (FD) approach where for each given frequency of interest, an elliptic partial differential equation is solved. Time domain (TD) approaches, on the other hand, can obtain the entire spectrum with the solution to a temporally short (and frequency rich) pulse. Beside circumventing the solution to multiple FD analyses, the possibility of having a linear solution complexity in terms of number of elements for the TD approaches can result in a very efficient approach to obtain the entire spectrum of scattering parameters. In contract, the global coupling implied by the elliptic nature of FD approach means that as the problem size (number of element) increases, the solution cost of even one FD solution grows more rapidly than a TD solution, as corroborated by results reported in [1].

1.2 Discontinuous Galerkin method

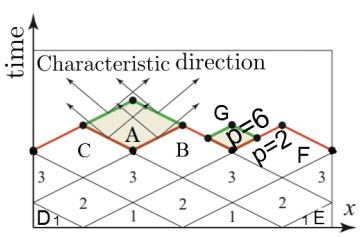

Figure 2. Spacetime discretization used in the SDG method.

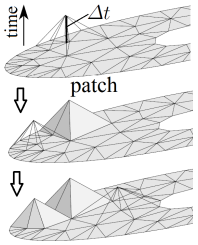

Figure 3. Patch-by-patch solution procedure.

The *spacetime discontinuous Galerkin* (SDG) method is a discontinuous Galerkin (DG) method that directly discretizes the spacetime using unstructured grids. Many exceptional properties of the method stem from the use of *causal* meshes. For example in fig. 2 the solution of element A depends only on the solution of earlier elements B and C given that the red facets are causal (fastest waves shown in arrows only pass in one direction through the facet). The level-1 elements depend only on initial conditions and boundary conditions for the elements D and E. The level-1 element solutions can be computed locally. Thus, causal SDG meshes enable asynchronous, element-by-element solutions with linear solution complexity. For more information the readers are referred to [2].

We replace the individual elements in the $1d\times$time with small clusters of simplicial elements called *patches*, where only the exterior patch facets need to be causal as shown in fig. 3 for clusters of tetrahedral elements in $2d\times$time. Using an advancing-front procedure, in each step the *Tent Pitcher* algorithm advances in time a vertex in the *front mesh* to de-

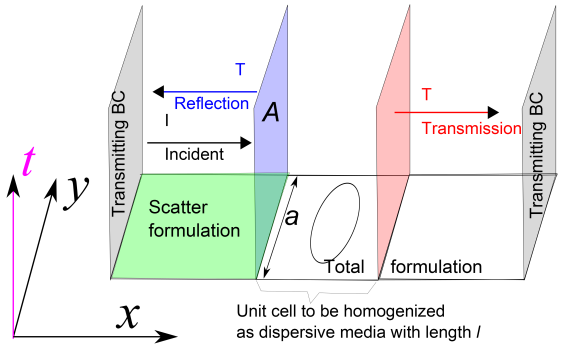

Figure 4. The schematic of time domain analysis for the derivation of reflection and transmission coefficients.

fine a local front update; the causality constraint limits the maximum time increment Δt at the vertex. We solve new patches as local problems and update the current front, until the entire spacetime analysis domain is solved.

An adaptive implementation of the method is presented in [3]. Some very unique aspects of our adaptive scheme are as follows: 1) as any other DG method there is no problem in having nonconforming elements of suddenly changing the element size as both cases are shown for element G in fig. 3; unlike conventional finite element methods no special transition elements are required; 2) the adaptivity decisions are local and do not need discarding the solution of all elements if a few ones have unacceptable errors. Also, by using special spacetime elements we replace space-only operations such edge-flip, vertex motion and mesh smoothing, and coarsening that would otherwise induce some projection errors between the old front and new front after adaptive operations. 3) The most interesting aspect is direct spacetime nature of our adaptive operations. For example, if the spatial size of an element decreases, its temporal size is automatically decreased by causality of the element; *cf.* element G in fig. 3. So the adaptive operation is both in space and time. In fact, our adaptive simulations often result in refinement ratios (ratio of domain to the smallest element size) of order 10^4 or larger in both space and time; *cf.* [3]. Moreover, arbitrarily high temporal orders of accuracy can be assigned at individual element level. In contrast, many existing adaptive schemes only adapt the mesh spatially and are very restrictive in having different time advances or interpolation orders in time due to their synchronous and often low temporal order of time marching scheme used.

2 Formulation and procedure

2.1 TD simulation of a short pulse

Figure 4 shows a schematic of the domain and boundary conditions used for the determination of reflection and transmission coefficients of a unit cell. The unit cell is illuminated by an planar wave $I(t)$ with the following properties: the FD response is broadband and the solution at initial and final times $t_0 = 0$, $\bar{T}$ is zero. The latter two properties enable to start the simulation from convenient zero initial condition and to have truncated integration interval for Fourier integrals: $\overline{f}(\omega) = \int_{-\infty}^{\infty} f(t)e^{-j\omega t}\,\mathrm{d}t \approx \int_0^{\bar{T}} f(t)e^{-j\omega t}\,\mathrm{d}t$. A Gaussian pulse, commonly used in spectral analysis in TD, is expressed as,

$$I(t) = \sin(\omega_0 t)e^{-(t-t_0)^2/\varsigma^2} \quad \Rightarrow \tag{1a}$$

$$\bar{I}(\omega) = \frac{1}{2} j\varsigma e^{-j\omega t_0}\left[e^{-\frac{\varsigma^2}{2}(\omega+\omega_0)^2} - e^{-\frac{\varsigma^2}{2}(\omega-\omega_0)^2}\right] \tag{1b}$$

where t_0 and ς are two time scales and ω_0 is a reference frequency. It is clear that the main frequency content of $\bar{I}(\omega)$ is in between $[\omega_{\min}, \omega_{\max}] = [\omega_0 - 1/\varsigma, \omega_0 + 1/\varsigma]$. If the range of frequencies of interest is known, ς and ω_0 are set by $\omega_0 = 0.5(\omega_{\max} + \omega_{\min})$ and $\varsigma = 2/(\omega_{\max} - \omega_{\min})$. The time t_0 is set such that at initial time $t = 0$, $I(t)$ is so weak that a zero initial condition everywhere is a very acceptable approximation. We often choose $t_0 \approx 3\varsigma$. The final time of TD simulation $\bar{T}$ is again chosen such that both $I(t)$ and the reflection of waves are well attenuated by absorption in the unit cell and/or transmission from the two sides of it.

We use the total field / scatter field (TF/SF) formulation by using SF for the side from which the incident wave is propagating from and TF in the unit cell and the zone following it. This permits using transmitting boundary conditions on the top and bottom of the domain to terminate the otherwise infinite span of the domain in that direction. We use Silver-Müller condition to terminate the domain. For the left and right sides of the domain we can use periodic boundary condition, but for the problems considered the unit cell is symmetric in the y-direction, facilitating the use of simpler boundary conditions that are implied by such symmetry.

2.2 Derivation of scattering parameters

The reflection coefficient in FD is obtained by computing the spatial average of $\overline{R}(\omega, y) \approx \int_0^{\bar{T}} R(t,y)e^{-j\omega t}\mathrm{d}t$, where $R(t,\mathbf{x})$ is the reflected wave measure on the scatter side of interface A in fig. 4. This spatial average is hence equal to $\overline{R}(\omega) = \frac{1}{a}\int_0^a \overline{R}(\omega, y)\mathrm{d}y = \frac{1}{a}\int_A R(t,y)e^{-j\omega t}\mathrm{d}A$. This integration is computed on triangular faces on A on the scatter side. We also compute the higher spatial components of solution by using certain orthonormal basis in y, but these terms are not relevant to the present study. The same computation is done on the transmission side. For the problems reported here, the incident, reflected, and transmitted waves are measured by E_z as a Transverse Magnetic (TM) mode is considered. The generalization to 3D and other propagation modes is straightforward. Finally, the reflection and transmission coefficients are computed as,

$$\bar{r}(\omega) = \frac{\overline{R}(\omega)}{\bar{I}(\omega)}, \quad \bar{t}(\omega) = \frac{\overline{R}(\omega)}{\bar{I}(\omega)} \tag{2}$$

2.3 Derivation of effective properties

If a medium with impedance Z and wave speed c is inserted between an ambient medium with permittivity ε_0 and per-

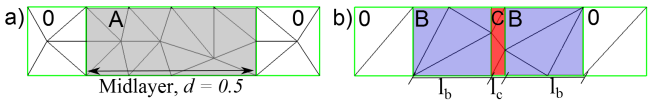

Figure 5. Initial meshes and schematics for a) a dispersive mid-layer A, b) 3-layer set BCB of materials B and C.

meability μ_0, its scattering parameters are derived by using two matching matrices (M1, M2) at the interfaces and one propagation matrix (P) as shown in fig. 1a) to obtain,

$$r = \rho \frac{z^2 - 1}{z^2 - \rho^2}, \quad t = z. \frac{1 - \rho^2}{z^2 - \rho^2} \tag{3}$$

where $\rho = (Z - Z_0)/(Z + Z_0)$ is the reflection coefficient at the left interface and $Z_0 = \sqrt{\mu_0/\varepsilon_0}$ is the impedance of the ambient. The parameter z is $z = e^{jkl}$, where $k = \omega/c$ is the wavenumber of wave in the medium and l is its length; *cf.* fig. 4. There are many studies on the inversion of (3) to obtain Z and c once r and t are known, for example from (3). We follow the process given by [4], where Z and z are obtained from,

$$Z = Z_0 \sqrt{\frac{(r+1)^2 - t^2}{(r-1)^2 - t^2}}, \quad z = \frac{(Z + Z_0) - r(Z - Z_0)}{t(Z + Z_0)} \tag{4}$$

As discussed thoroughly in [4], various choices of square root and solution options for z all result in the same eventual solutions for effective material properties. However, when deriving k from $z = e^{jkl}$ by a log operator we observe,

$$k = \frac{\phi}{l} - j\frac{\log \rho}{l}, \quad \text{where} \quad \phi := \theta + 2p\pi \tag{5}$$

and ρ and $\theta \in [0, 2\pi)$ are used in polar expression of $z = \rho e^{j\theta}$. The integer p is the only source of ambiguity in determining phase angle ϕ. This implies that any integer number of waves traversed in middle medium can be added without changing scattering properties which makes physical sense. As discussed in [4], p can be set to zero for very small frequencies and correct value be assigned as ω increases by maintaining continuity of effective material properties. However, our studies demonstrate that maintaining continuity of phase angle $\phi = \theta + 2p\pi$ as ω increases is a more robust approach, especially for highly dispersive media to be characterized. Finally, once correct value of k is set, noting that $c = \omega/k = 1/\sqrt{\varepsilon\mu}$ and $Z = \sqrt{\frac{\mu}{\varepsilon}}$ the effective properties are obtained by,

$$\varepsilon = \frac{k}{Z\omega}, \quad \mu = \frac{kZ}{\omega} \tag{6}$$

3 Numerical Results

Figure 5 shows the schematic of the unit cell and the intial meshes used for two problems considered herein. For both problems we use $\varepsilon_0 = 1$ and $\mu_0 = 1$ for the material on the two sides of unit cell. Figure 5a) corresponds to a microscale homogeneous material for which the unit

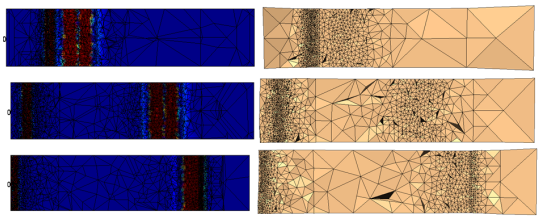

Figure 6. Solution (left) and space front (right) of the wave propagation in the media at different times.

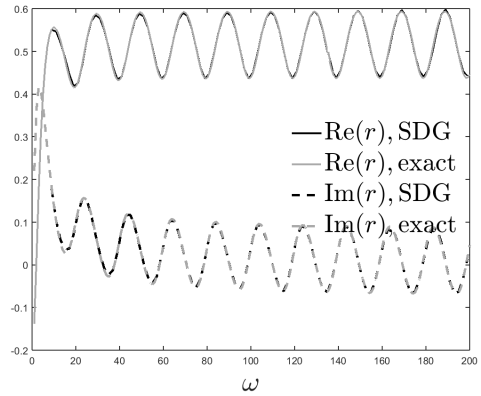

Figure 7. Comparison of the computational and exact reflection coefficient.

cell is composed of material A with parameters $\varepsilon_A = 0.1$, $\mu_A = 1$, and conductivity $\sigma_A = 1$. The goal is to successfully retrieve the material properties for the unit cell. Figure 6 shows a few snapshots of the solution, color shows E_z, and the front mesh as the incident wave reflect and transmit from the two interfaces and pass through the medium (results are presented for a case where $\sigma_A = 0$ to better demonstrate moving wave fronts). As it can be seen the refinement operations create smaller elements at the wave fronts where larger numerical dissipations are encountered. Once the wave front passes a region, spacetime adaptive operations coarsen the front to reduce computational costs. It is also interesting to note the difference between the front mesh at different times and the initial mesh front in fig. 5a).

Figure 7 compares the computational and exact real and imaginary parts of reflection coefficient. The computational results are obtained by the Fourier transform of TD data as described in §2.1 and §2.2 while the exact solution are computed from (3). It can be seen that there is a very good match between computational and exact results.

Once scattering parameters are computed, we can use the inverse parameter retrieval procedure from §2.3 to obtain the effective ε and μ for the unit cell. One critical step is obtaining the correct integer p for computing the wavenumber k in (5). Figure 8 depicts p and phase ϕ, divided by 2π, for the range of frequencies considered. Finally, fig. 9 shows the real part of ε retrieved by using (6) which is indistinguishable from the exact value of $\varepsilon(\omega) = \varepsilon_A + \sigma_A/(j\omega)$ for the range $\omega \in [0,\ 200]$. From §2.3 it is evident that the maximum frequency corresponds to a slightly more than 5 full cycles of wave in the unit cell. The frequency for one full cycle is $\omega = 2\pi c_A/l = 2\pi \times 1/\sqrt{0.1}/0.5 = 39.74$.

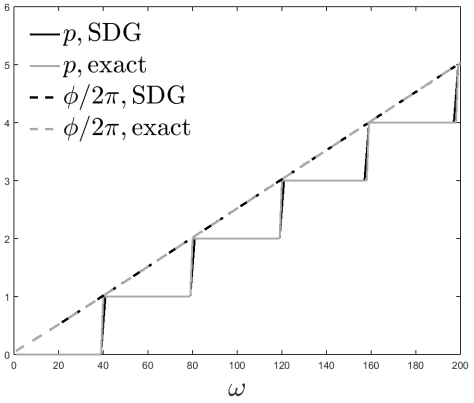

Figure 8. Integer p and scaled phase $\phi/2\pi$ obtained in inverse parameter retrieval stage.

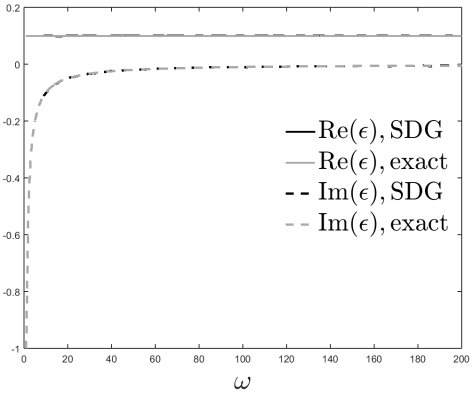

Figure 9. Real and imaginary parts of retrieved and exact permittivity $\varepsilon(\omega)$ for $\omega \in [1,\ 200]$.

The second example corresponds to the set-up in fig. 5b) where two materials B and C with properties $\varepsilon_B = 0.1$, $\mu_B = 1$ and $\varepsilon_C = 1$, $\mu_C = 1$, $\sigma_C = 1$ are considered. The thickness of layers are $l_b = 0.23$ and $l_c = 0.04$. The retrieved phase values are compared in fig. 10. There is a very good agreement between the exact and computational values. It should be emphasized that retrieved p is not necessarily increasing due to discretization and finite precision errors but imposing the continuity and monotonicity of phase value ϕ is critical in retrieving correct material parameters. Finally, in fig. 11 the real part of dispersive permittivity $\varepsilon(\omega)$ are compared. In general, there is

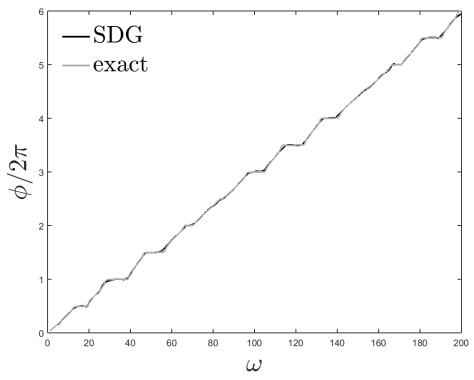

Figure 10. Comparison of the exact and computational scaled phase $\phi/2\pi$ for the 3 layer unit cell.

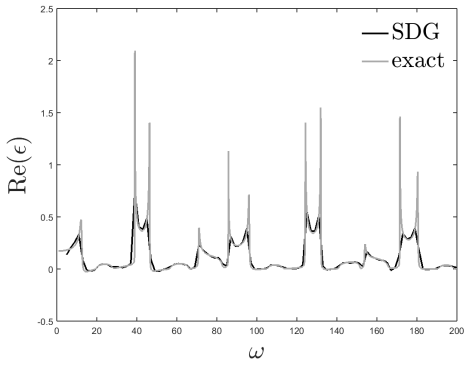

Figure 11. Real part of computational and exact permittivity $\varepsilon(\omega)$ for the 3 layer unit cell and $\omega \in [1,\ 200]$.

a good agreement between numerical and exact solutions, however, by tightening the adaptivity tolerance we can have a better match at resonance frequencies.

4 Conclusions

We presented an adaptive TD approach that can effectively obtain scattering parameters and effective properties of a unit cell with only one TD simulation. The homogenization to an effective medium is physically only meaningful for the lower range of frequencies reported for example for the second problem. However, it is demonstrated that the FD scattering parameters obtained from the SDG TD solution and the subsequent inverse parameter retrieval method are robust and accurate for a wide range of frequencies. We will also present some results for the characterization of nontrivial 2D unit cells at the GASS 2017 conference.

References

[1] K. Busch, M. Konig, and J. Niegemann. Discontinuous Galerkin methods in nanophotonics. *Laser Photonics Reviews*, 5(6):773–809, 2011.

[2] Reza Abedi, Robert B. Haber, and Boris Petracovici. A spacetime discontinuous Galerkin method for elastodynamics with element-level balance of linear momentum. *Computer Methods in Applied Mechanics and Engineering*, 195:3247–3273, 2006.

[3] R. Abedi, R. B. Haber, S. Thite, and J. Erickson. An *h*–adaptive spacetime–discontinuous Galerkin method for linearized elastodynamics. *Revue Européenne de Mécanique Numérique (European Journal of Computational Mechanics)*, 15(6):619–642, 2006.

[4] S Arslanagić, T. V. Hansen, N. A. Mortensen, A. H. Gregersen, O. Sigmund, R. W. Ziolkowski, and O. Breinbjerg. A review of the scattering-parameter extraction method with clarification of ambiguity issues in relation to metamaterial homogenization. *IEEE Antennas and Propagation Magazine*, 55(2):91–106, 2013.